Author Manuscript

Author Manuscript

Author Manuscript

Author Manuscript

HHS Public Access

Author manuscript

Curr Biol. Author manuscript; available in PMC 2022 July 12.

Published in final edited form as:

Curr Biol. 2021 July 12; 31(13): 2895–2905.e7. doi:10.1016/j.cub.2021.04.075.

Rab34 GTPase mediates ciliary membrane formation in the intracellular ciliogenesis pathway

Anil Kumar Ganga[1], **Margaret C. Kennedy**[1], **Mai E. Oguchi**[2], **Shawn Gray**[3], **Kendall E. Oliver**[1], **Tracy A. Knight**[1], **Enrique M. De La Cruz**[3], **Yuta Homma**[2], **Mitsunori Fukuda**[2], **David K. Breslow**[1,*]

[1]Department of Molecular, Cellular, and Developmental Biology, Yale University, New Haven, CT 06511, USA

[2]Laboratory of Membrane Trafficking Mechanisms, Department of Integrative Life Sciences, Graduate School of Life Sciences, Tohoku University, Aobayama, Aoba-ku, Sendai, Miyagi 980-8578, Japan

[3]Department of Molecular Biophysics and Biochemistry, Yale University, New Haven, CT 06511, USA

Summary

The primary cilium is an essential organizing center for signal transduction, and ciliary defects cause congenital disorders known collectively as ciliopathies.[1–3] Primary cilia form by two pathways that are employed in a cell type- and tissue-specific manner: an extracellular pathway in which the cilium grows out from the cell surface and an intracellular pathway in which the nascent cilium first forms inside the cell.[4–8] After exposure to the external environment, cilia formed via the intracellular pathway may have distinct functional properties, as they often remain recessed within a ciliary pocket.[9],[10] However, the precise mechanism of intracellular ciliogenesis and its relatedness to extracellular ciliogenesis remain poorly understood. Here we show that Rab34, a poorly characterized GTPase recently linked to cilia[11–13], is a selective mediator of intracellular ciliogenesis. We find that Rab34 is required for formation of the ciliary vesicle at the mother centriole and that Rab34 marks the ciliary sheath, a unique sub-domain of assembling intracellular cilia. Rab34 activity is modulated by divergent residues within its GTPase domain, and ciliogenesis requires GTP binding and turnover by Rab34. Because Rab34 is found on assembly

*Lead Contact: David K. Breslow, david.breslow@yale.edu 203-432-8280, Yale Science Building, Room 216, 260 Whitney Ave, New Haven, CT 06511.

Author Contributions

Anil Kumar Ganga and Margaret C. Kennedy designed and conducted most experiments and analyzed results. Mai E. Oguchi, Yuta Homma, and Mitsunori Fukuda analyzed ciliogenesis in MDCK cells. Kendall E. Oliver analyzed Rab34 mutants, and Tracy A. Knight conducted expansion microscopy. Shawn D. Gray developed the recombinant protein purification protocol and performed biochemical analyses with purified protein components under the supervision of Enrique M. De La Cruz. David Breslow designed experiments, analyzed results, and supervised the project. David K. Breslow and Anil Kumar Ganga wrote the manuscript with input from all authors.

Declaration of interests

The authors declare no competing financial interest.

Publisher's Disclaimer: This is a PDF file of an unedited manuscript that has been accepted for publication. As a service to our customers we are providing this early version of the manuscript. The manuscript will undergo copyediting, typesetting, and review of the resulting proof before it is published in its final form. Please note that during the production process errors may be discovered which could affect the content, and all legal disclaimers that apply to the journal pertain.

Author Manuscript Author Manuscript Author Manuscript Author Manuscript

intermediates that are unique to intracellular ciliogenesis, we tested its role in the extracellular pathway used by polarized MDCK cells. Consistent with Rab34 acting specifically in the intracellular pathway, MDCK cells ciliate independently of Rab34 and its paralog Rab36. Together, these findings establish that different modes of ciliogenesis have distinct molecular requirements and reveal Rab34 as a new GTPase mediator of ciliary membrane biogenesis.

eTOC Blurb:

Different cell types form primary cilia through different assembly pathways. Ganga et al. show that the GTPase Rab34 is needed for ciliary membrane formation in the intracellular ciliogenesis pathway but not the extracellular pathway. During intracellular ciliogenesis, Rab34 is recruited to nascent cilia and localizes to the ciliary sheath.

Graphical Abstract

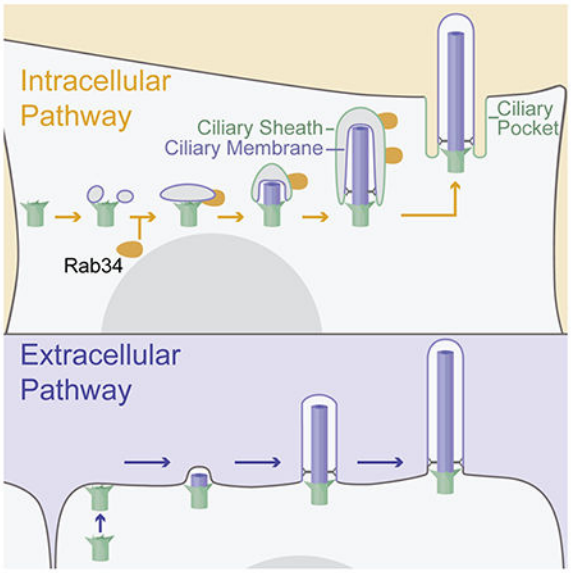

Keywords

cilia; ciliogenesis; ciliopathy; centriole; GTPase; membrane; ciliary vesicle; Rab

Results

Rab34 is required for ciliogenesis

We and others recently identified *Rab34* as a hit in genome-wide screens for regulators of cilium-dependent Hh signaling.[11,14] Our CRISPR screen was based on an NIH-3T3 reporter cell line in which a blastidicin resistance gene is induced in response to Hh pathway activation. Notably, *Rab34* was a top-scoring hit, with all ten *Rab34*-targeting sgRNAs causing decreased resistance to blasticidin[14] (Figure 1A). We used two of these sgRNAs to generate *Rab34* mutant NIH-3T3 cell pools and observed strongly reduced ciliogenesis, as assessed by ARL13B or acetylated tubulin staining (Figures 1B–C and S1A). We also

Author Manuscript Author Manuscript Author Manuscript Author Manuscript

knocked out *RAB34* in RPE1 cells, a widely used model for ciliogenesis. We used two *RAB34*-targeting sgRNAs and generated clonal and polyclonal cell lines with frame-shift mutations and/or strongly reduced levels of Rab34 protein (Figure S1B). As in NIH-3T3 cells, ciliogenesis was greatly reduced in RPE1 *RAB34* mutants (Figures 1D and S1C–D). Additionally, expression of human *RAB34* rescued ciliogenesis in *Rab34* mutant NIH-3T3 cells, confirming the specificity of the mutant phenotype (Figure 1G).

Rab34 GTP binding and hydrolysis are necessary for ciliogenesis

Rab GTPases cycle between an inactive GDP-bound state and an active GTP-bound state, and mutations at conserved residues can be used to alter this nucleotide cycle[15–19] (Figure 1E). In the case of Rab34, a Q111L mutation is predicted to block GTP hydrolysis and lock Rab34 in the GTP-bound state, while a T66N mutation is expected to impair GTP binding (Figure 1E–F). We transfected *Rab34* mutant NIH-3T3 cells with GFP-tagged Rab34 constructs and found that Rab34-WT and Rab34-Q111L efficiently rescued the ciliogenesis defect while Rab34-T66N did not. Thus, GTP-binding by Rab34 is essential for ciliogenesis (Figure 1G).

While analyzing the sequence of Rab34, we noted two residues—Leu61 and Ser166—that are conserved within Rab34 orthologs but diverge from the amino acids typically seen in Rab GTPases (Figures 1F and S1E). These residues are likely to be functionally important, as Leu61 lies in the P-loop and corresponds to Gly12 of KRAS, where G12D is a common oncogenic mutation.[20] Ser166 is typically an asparagine in the NKxD motif, and mutations at this position impair nucleotide binding.[21,22] We therefore examined ciliogenesis in *Rab34* mutant cells expressing Rab34-S166N (reverting Ser166 to Asn) and Rab34-L61D (mimicking KRAS-G12D). Notably, both mutants failed to rescue ciliogenesis in *Rab34* mutant cells (Figure 1G) and appeared to reduce ciliogenesis in wildtype cells (not shown). To further examine this dominant-negative effect, we generated RPE1 cell lines with doxycycline-inducible GFP-Rab34-WT, L61D, and S166N. While cells over-expressing wildtype Rab34 assembled cilia efficiently, induction of Rab34-L61D or Rab34-S166N caused a severe ciliogenesis defect (Figure 1H).

To determine how the S166N and L61D mutations affect the nucleotide cycle of Rab34, we analyzed Rab34-bound nucleotides in HEK293T cells that were transfected with GFP-tagged Rab34 variants and metabolically labeled with ^{32}P-phosphate. Consistent with an earlier report[23], wildtype Rab34 was mostly GDP-bound. However, Rab34-S166N and Rab34-L61D both bound more GTP, suggesting that these are GTP-locked mutants (Figure 1I). By contrast, the Q111L mutant canonically predicted to be GTP-locked was similar to wildtype, possibly because such Rab mutants can remain susceptible to GAP-stimulated GTP hydrolysis.[24] Increased GTP binding by Rab34-S166N and Rab34-L61D is further supported by co-immunoprecipitation experiments in which these mutants exhibit increased binding to RILPL1, a putative effector that recognizes the GTP state[25,26], and decreased binding to Rab-GDI, a binding partner selective for the GDP state[18] (Figure S1F). Lastly, we examined how these mutations affect the GTPase activity of purified recombinant Rab34. Notably, Rab34-L61D exhibited a ~100-fold lower k_{cat} than wildtype Rab34 and a ~100-fold tighter K_m for GTP, while GTPase activity for Rab34-S166N was below our limit of

Author Manuscript Author Manuscript Author Manuscript Author Manuscript

detection (Figure S1G). These findings support our cell-based studies and indicate that GTP binding and hydrolysis by Rab34 are required for ciliogenesis.

Rab34 mediates ciliary vesicle formation

The intracellular ciliogenesis pathway used by NIH-3T3 and RPE1 cells involves a number of sequential steps and requires dynamic recruitment of proteins including MYO5A, EHD1, and Rab8 (Figures 2A and S2A). One of the earliest events is transport of pre-ciliary vesicles to the mother centriole by MYO5A, where they are captured at the distal appendages to give rise to MYO5A-labeled Distal Appendage Vesicles (DAVs).[7,8,27] These events appear to occur normally in *RAB34* mutant cells, as distal appendages marked by CEP164 are present, and MYO5A is recruited to the mother centriole (Figure 2B–C). After DAVs are captured at the mother centriole, they fuse into a larger ciliary vesicle through the action of EHD family ATPases.[6,7] Notably, *RAB34* knockout cells exhibited a significant defect in recruitment of EHD1-mScarlet-I to the mother centriole (Figure 2D). A similar defect was observed for GTPases Rab8 and ARL13B (Figures 2E and S1C), which are recruited after EHD1 to promote ciliary membrane growth.[28,29] To directly observe the membrane remodeling events that occur during intracellular ciliogenesis, we used Focused Ion Beam Scanning Electron Microscopy (FIB-SEM). Strikingly, 3D reconstructions from *RAB34* mutant cells consistently revealed multiple small vesicles docked to the distal appendages without any evident ciliary vesicle (seen for 7 *RAB34* knockout cells analyzed; for 2 additional cells, details were obscured by neighboring organelles; Figures 2G and S2C). Thus, DAVs are recruited normally in *RAB34* mutant cells, but fusion of DAVs to form a ciliary vesicle is defective, a phenotype similar to that seen upon *EHD1* knockdown.[7]

In addition to ciliary membrane formation, ciliogenesis requires removal of capping protein CP110 from the mother centriole and recruitment of the intraflagellar transport (IFT) complexes IFT-A and IFT-B (Figure 2A).[30] In *RAB34* mutant cells, CP110 was removed normally, and IFT88 (IFT-B) and IFT140 (IFT-A) were still present at mother centrioles (Figures 2F, 2H–I, and S2A–B).

We next evaluated cells expressing dominant-negative Rab34 and found that, as in *RAB34* knockout cells, Rab34-S166N did not inhibit CEP164 localization, CP110 removal, or IFT complex recruitment (Figure S2D–G). FIB-SEM reconstructions showed that cells expressing Rab34-S166N also arrested ciliogenesis with DAVs docked to the mother centriole (5 of 6 cells examined). However, the DAVs displayed a striking elongated or tubular morphology (Figures 2J and S2C). This finding strongly suggests that Rab34 acts directly on DAVs and that Rab34-S166N alters membrane fusion or remodeling at the mother centriole.

The ability to inducibly express Rab34-S166N allowed us to examine the effect of disrupting Rab34 function after cilium assembly. Interestingly, progressive loss of cilia was observed after induction of Rab34-S166N but not Rab34-WT (Figure S2H–I). Rab34 is therefore also needed to maintain cilia in cultured cells. Moreover, treating cells with the actin poison cytochalasin D (cytoD) rescued this defect. Thus, the ability of cytoD to stabilize cilia[31] bypasses the need for Rab34 in cilium homeostasis (Figure S2J).

Author Manuscript Author Manuscript Author Manuscript Author Manuscript

Rab34 dynamically localizes to the mother centriole and cilium during ciliogenesis

Because Rab GTPases are recruited to the membrane structures they regulate, we next examined Rab34 localization. Notably, staining with two antibodies revealed colocalization of Rab34 with ciliary markers in ~10% of ciliated RPE1 cells (Figures 3A and 3D). We also commonly observed a punctum of Rab34 at the mother centriole in unciliated cells, and similar localizations were observed in NIH-3T3 cells (Figure 3A–B). In serum-fed, sub-confluent RPE1 cells, ~12% of mother centrioles were Rab34-positive, while ~35% of mother centrioles became Rab34-positive early during ciliogenesis (Figures S3A and 3C). At this stage (4 h after serum starvation), only ~10% of mother centrioles were marked by ARL13B, suggesting that Rab34 is recruited before ARL13B (Figure 3C). By contrast, at later timepoints, the fraction of cilia with Rab34 decreased (Figure 3D). Thus, Rab34 may act early during ciliogenesis and be selectively present on nascent cilia.

To further understand Rab34 localization dynamics, we carried out live-cell imaging in cells stably expressing ARL13B-mScarlet-I, miRFP-670-Centrin2, and GFP-Rab34. By directly monitoring cilium assembly, we observed, first, that all ciliating cells dynamically recruited Rab34 to the mother centriole during ciliogenesis (Figure 3E–F). Second, Rab34 consistently arrived at the mother centriole before ARL13B. Third, most cells exhibited dynamic ciliary localization of Rab34 after an ARL13B-positive cilium formed. Overall, the Rab34 localization dynamics we observed are consistent with a key role for Rab34 in ciliary membrane formation.

We also examined the localization of dominant-negative GFP-Rab34-S166N and GFP-Rab34-L61D and found that these proteins localized as a bright punctum at the mother centriole in ~90% of cells (Figures 3G and S3B). Given that these cells also exhibit distended DAVs (Figure 2J), it is likely that Rab34 is present on DAVs and that GTP-locked mutants become trapped on these structures, impairing DAV fusion.

Rab34 localization and function are specific to intracellular ciliogenesis

Because Rab34 is found on a subset of cilia that declines during the course of ciliogenesis (Figure 3D), we next asked whether Rab34 localizes to nascent intracellular cilia. To distinguish nascent intracellular (‘inside’) cilia from mature extracellular (‘outside’) cilia, we used the In/Out assay.[32] Specifically, we used an anti-GFP Nanobody (Nb)[33] to stain pHluorin-Smo in surface-exposed cilia of live cells, followed by fixation and anti-Rab34 immunostaining. Strikingly, even though most cilia were extracellular after 48 h of serum-starvation, all Rab34-positive cilia were negative for GFP Nb staining and therefore intracellular (Figure 4A–B). Furthermore, Rab34 localized to the majority of inside cilia (Figure S3C), indicating that Rab34 is a GTPase marker of intracellular cilia. We note that similar results were also obtained with an antibody-based In/Out assay protocol (Figure S3D–E). Thus, Rab34 localizes to a small fraction of cilia because it is found selectively on nascent intracellular cilia.

Intracellular cilia possess two adjacent membrane domains: the ciliary membrane and the surrounding ciliary sheath (Figure 2A). To determine which of these membranes harbors Rab34, we used 3D structured illumination microscopy (3D-SIM). Notably, Rab34

Author Manuscript Author Manuscript Author Manuscript Author Manuscript

fluorescence consistently surrounded the ARL13B-labeled ciliary membrane (Figures 4C and S3F), as reported for ciliary sheath proteins such as EHD1 and MYO5A.[8] We obtained similar results using expansion microscopy, in which samples are embedded in a swellable polymer to allow ~4-fold isotropic expansion.[34,35] In expanded samples, Rab34 fluorescence surrounded ARL13B, with polyE-tubulin marking the center of the cilium (Figures 4D and S3G). These results establish that Rab34 localizes to the ciliary sheath and identify Rab34 as the first GTPase enriched on the ciliary sheath. Notably, although the sheath is a precursor to the ciliary pocket, Rab34 was largely absent from the ciliary pocket in RPE1 cells, as 25 of 26 EHDl-positive ciliary pockets lacked Rab34 staining (Figure S3H).

Because Rab34 localizes to structures unique to intracellular ciliogenesis, we hypothesized that Rab34 might be dispensable for extracellular ciliogenesis. As a model of extracellular ciliogenesis, we used the epithelial Madin-Darby Canine Kidney II (MDCK) cell line. During cilium assembly in MDCK cells, the mother centriole migrates to the apical surface before ciliary membrane formation, and intracellular intermediates are not readily detected by the In/Out assay.[10,36,37] We used CRISPR to target *Rab34* and its paralog *Rab36* in MDCK cells and confirmed knockout by Western blot and DNA sequencing[38] (Figure S4A). Consistent with our hypothesis, we did not observe any ciliogenesis defect in *Rab34* mutant MDCK cells grown in 3D cysts or polarized 2D monolayers, nor did we observe any change in cilium length (Figures 4E, 4G and, S4B). *Rab34/Rab36* double-knockout cells also exhibited normal cilia, ruling out the possibility that Rab34 and its paralog Rab36 function redundantly in MDCK ciliogenesis (Figure 4E–G). Finally, while Rab34 is expressed in MDCK cells, we did not observe Rab34 localization at cilia or centrioles in ciliating MDCK cells (Figures S4A and S4C). Thus, extracellular ciliogenesis in MDCK cells is independent of Rab34 and Rab36.

Discussion

Here, we found that Rab34 is a key mediator of ciliary membrane formation in the intracellular ciliogenesis pathway (Figure 4H). While Rab34 was recently suggested to promote early stages of ciliary membrane formation and to localize to some cilia[12,13], we now show that Rab34 mediates ciliary vesicle formation and is specifically found on the ciliary sheath of intracellular cilia. Rab34 is also dynamically recruited to the mother centriole during ciliogenesis, and the persistent localization of Rab34-S166N at this site suggests that Rab34 is present on DAVs (Figure 3C–G). Rab34 may therefore establish the membrane identity of DAVs and the ciliary sheath. Because the ciliary sheath faces the cytoplasm, Rab34 may also promote vesicular trafficking to the nascent cilium and/or fusion of the ciliary sheath with the plasma membrane. Additionally, Rab34 may have a role in membrane trafficking to mature cilia given the impairment of cilium maintenance seen upon Rab34-S166N expression. A clearer picture of Rab34's roles beyond DAV fusion awaits the development of tools to rapidly inactivate Rab34 during ciliogenesis. How Rab34's localization is dynamically regulated will also be an important area for future study.

Rab34 is an atypical GTPase with key residues that differ from other family members. These divergent residues have critical roles, as Rab34-S166N and Rab34-L61D are GTP-locked

Author Manuscript Author Manuscript Author Manuscript Author Manuscript

dominant-negative mutants that block ciliogenesis (Figures 1H–I and S1F–G). Further insight into the Rab34 enzymatic cycle and the impact of these mutations awaits the identification of GEFs and GAPs that regulate Rab34. Similarly, Rab34's effectors that mediate ciliogenesis remain unknown. We anticipate that the GTP-locked Rab34 mutants identified here will be valuable tools to uncover Rab34 effectors and regulators.

Our data indicate that cells using the extracellular pathway can form cilia independently of Rab34 (Figure 4E–G). It remains unclear if other proteins such as EHD1 and MYO5A also have selective roles in intracellular ciliogenesis. Both proteins promote ciliogenesis in RPE1 and IMCD3 cells, and *Ehd* gene knockdown in zebrafish impacts cilia in some epithelial tissues. However, mice lacking these proteins exhibit no (or variable) ciliary defects, and their roles have not yet been examined in MDCK cells.[7,8,39–43] A pathway-specific role for Rab34 is nonetheless consistent with the fact that, unlike many genes needed for ciliogenesis, *Rab34* is not conserved in all ciliated organisms but is restricted to metazoans.[44] Indeed, one possibility is that Rab34 is selectively present in organisms that employ the intracellular ciliogenesis pathway.

Lastly, our findings provide a framework for understanding the physiologic roles of Rab34 and the consequences of its inactivation. Homozygous *Rab34* mutant mice die perinatally and exhibit ciliopathy features such as polydactyly and craniofacial malformations.[12,45] However, these phenotypes are milder than the early embryonic lethality seen for mutants that cause universal cilium loss[46] and are instead consistent with disruption of a subset of ciliated tissues. For example, neural tube patterning is apparently normal in some *Rab34* mutant embryos, which is consistent with these epithelial cells lacking a pronounced ciliary pocket and likely ciliating via the extracellular pathway.[47–49] Conversely, limb buds of *Rab34* mutant mice exhibit polydactyly and have fewer cilia.[12] It is noteworthy that cells of the limb bud mesenchyme have a pronounced ciliary pocket and likely ciliate via the intracellular pathway.[50] Cerebellar granule neuron progenitors also likely ciliate via the intracellular pathway[51], and the limb bud and cerebellum are both tissues where *Rab34* is induced by Hh signaling.[52,53] Although the functional significance of *Rab34* induction is unclear, one possibility is that Rab34 promotes cilium re-formation after mitogenic Hh signaling, as recently reported for *Atohl*.[54] Finally, while patients with *RAB34* mutations have not yet been reported, understanding the clinical manifestations of *RAB34* disruption is likely to provide new insights into tissue-specific modes of cilium assembly and into the phenotypic variability seen in ciliopathies.

STAR Methods

RESOURCE AVAILABILITY

Lead Contact—Further information and requests for resources and reagents should be directed to and will be fulfilled by the Lead Contact, David Breslow (david.breslow@yale.edu).

Materials availability—All unique/stable reagents generated in this study are available from the Lead Contact.

Author Manuscript Author Manuscript Author Manuscript Author Manuscript

Data and code availability—Raw data not included in this article are available from the corresponding author on request.

EXPERIMENTAL MODEL AND SUBJECT DETAILS

Mammalian cell lines—NIH-3T3, RPE1-hTERT (RPE1), and HEK-293T cell lines were obtained from ATCC; MDCK-II cells were obtained from Katsuhiko Mikoshiba (ShanghaiTech University). Cultured cells were maintained in a humidified 37°C incubator with 5% CO_2. NIH-3T3, HEK-293T, and MDCK-II cells were cultured in DMEM, high glucose (Gibco) supplemented with 10% fetal bovine serum (FBS; Sigma Aldrich), 100 units/ml Penicillin, 100 μg/ml Streptomycin, 2 mM Glutamine, and 1 mM sodium pyruvate (Gibco). RPE1 cells were cultured in DMEM/F-12 medium (Gibco) supplemented with 10% FBS, 100 units/ml of Penicillin, 100 μg/ml Streptomycin, and 2 mM Glutamine. To induce ciliogenesis, NIH-3T3 cells were starved in 0.5% FBS-containing medium for 24 h, and RPE-1 cells were starved in 0.2% FBS-containing medium for 48 h. For analysis of ciliogenesis of MDCK cells grown in two-dimensional (2D) monolayers, cells were cultured until confluence was achieved (5 days after seeding). Three-dimensional (3D) MDCK cysts were formed by culturing cells in collagen I gel (KOKEN #IPC-50), as described previously.[38] Where specified, cells were treated with 100 nM cytochalasin D (Sigma Aldrich) or with 1 μg/ml doxycycline (Fisher Scientific). Cells were verified to be mycoplasma-negative using MycoAlert Plus detection kit (Lonza).

E. Coli—BL21(DE3) cells were used for recombinant protein expression and grown in LB medium.

METHOD DETAILS

DNA cloning—Gibson assembly, Gateway cloning, and standard molecular biology were used for DNA cloning. Human *RAB34* cDNA was obtained from GE Healthcare (MHS6278-202807876) and cloned into Gateway pENTR plasmid pDONR221 (Invitrogen); *RAB34* mutants were prepared by site-directed mutagenesis of pENTR-Rab34. Plasmids for tetracycline-inducible expression of LAP-Rab34 (LAP consists of GFP, TEV protease site, and S-tag) were constructed by modification of pCW-Cas9 (Addgene #50661, gift from Eric Lander and David Sabatini). Stable expression of fluorescently tagged ciliary and centriolar proteins was achieved by modification of pCW-Cas9 using cDNAs for the PGK promoter, ARL13B (Addgene #40879, gift from Tamara Caspary), EHD1 (gift from Chris Westlake), Rab8 (gift from Maxence Nachury), and Centrin2 (gift from Tim Stearns), miRFP-670 (Addgene #79987, gift from Vladislav Verkhusha), and mScarlet-I (Addgene #85044, gift from Dorus Gadella). Plasmids for CRISPR-based knockout were constructed using pMCB320 (Addgene #89359, gift from Michael Bassik) and pMJ179 (Addgene #89556, gift from Jonathan Weissman); see Key Resources Table for sgRNA sequences. Plasmids for transient transfection of *RAB34* were made by Gateway cloning using pEF5-FRT-LAP-DEST[55,56]; for bacterial protein expression, *RAB34* variants were cloned into pGEX-6P1 (GE Healthcare).

Lentivirus production and cell line generation—VSVG-pseudotyped lentiviral particles were produced by transfection of HEK293T cells with a lentiviral vector and

Author Manuscript Author Manuscript Author Manuscript Author Manuscript

packaging plasmids (pMD2.G, pRSV-Rev, pMDLg/RRE for sgRNAs; pCMV-ΔR-8.91 and pCMV-VSVG for protein-coding constructs). Following transfection using polyethyleneimine (Polysciences #24765-1), virus-containing supernatant was collected 48 h later and filtered through a 0.45 μm polyethersulfone filter (VWR 28145-505). For protein-coding constructs, lentiviral particles were concentrated 10-fold using Lenti-X Concentrator (Takara Biosystems).

Cells were transduced by addition of viral supernatants diluted to an appropriate titer in medium containing 4 mg/ml polybrene (Sigma Aldrich H9268). Following 24 h incubation at 37°C, virus-containing medium was removed, and cells were passaged and selected, as appropriate, using 2.0-8.0 μg/ml puromycin or 300 μg/ml G418 or 8.0 μg/ml blasticidin (InvivoGen). Alternatively, transduced cells were isolated by FACS using a FACSAria III sorter (Becton Dickinson). Unless otherwise indicated, polyclonal pools of transduced cells were used in subsequent experiments.

For CRISPR-based mutagenesis of NIH-3T3 cells, a cell line stably expressing Cas9 was used (3T3-[Shh-BlastR];Cas9).[14] For mutagenesis of RPE1 cells, a cell line stably expressing Cas9 was generated by infection with lentiCas9-Blast (Addgene #52962, gift from Feng Zhang) and selection with blasticidin. Cas9-expressing cells were transduced with sgRNA constructs followed by antibiotic selection or FACS-based sorting of clones. Mutant alleles in knockout clones were assessed by sequencing of genomic DNA extracted using the QIAamp DNA Mini kit (Qiagen). The target locus was amplified using flanking primers (see Key Resources Table) and subjected to Sanger sequencing. Generation of *Rab34, Rab36* and *Rab34/Rab36* knockout MDCK cells was described previously.[38]

Staining for immunofluorescence microscopy—Staining for immunofluorescence microscopy was performed as described previously [14]. Briefly, cells were seeded on acid-washed 12-mm #1.5 coverslips (Fisher Scientific). Cells were either fixed in 4% paraformaldehyde (Electron Microscopy Sciences) for 10 min or −20°C methanol for 10 min or 4% paraformaldehyde for 10 min followed by methanol or 10% TCA for 10 min (for MDCK cysts). Coverslips were permeabilized for 10 min in PBS containing 0.1 % Triton X-100, washed with PBS, and blocked for 20 min in PBS supplemented with 5% normal donkey serum (Jackson Immunoresearch) and 3% Bovine Serum Albumin (BSA). Coverslips were then incubated with appropriate primary antibodies diluted in PBS with 3% BSA at room temperature for 1 h, washed five times, incubated with secondary antibodies for 30-60 min at room temperature, washed again, stained with Hoechst 33258 dye, and mounted on glass slides in Fluoromount-G mounting medium (Electron Microscopy Sciences). MDCK cysts were transferred in PBS to glass-bottom dishes for imaging. Primary and secondary antibodies used are listed in the Key Resources Table.

In/Out Assay—In/Out Assay with anti-GFP antibody was carried out as described previously [32]. Briefly, coverslips were fixed in 4% paraformaldehyde for 10 min and blocked in PBS containing 5% normal donkey serum and 3% BSA for 20 min. After blocking, unpermeabilized coverslips were incubated with rabbit anti-GFP antibody for 30 min at room temperature. After washing, coverslips were fixed again in 4% paraformaldehyde, permeabilized with PBS containing 0.1% Triton X-100, blocked again,

Author Manuscript Author Manuscript Author Manuscript Author Manuscript

and incubated with anti-Rab34 antibody (SCBT) for 1 h at room temperature. Coverslips were then washed, stained with secondary antibodies, and mounted on glass slides as described above.

The In/Out Assay with anti-GFP nanobody (Nb) was based on a modified version of the above protocol. Coverslips were placed on ice, washed with cold HKM-E1 buffer (20 mM HEPES, pH 7.4, 115 mM KOAc, 1 mM $MgCl_2$, and 1 mM EGTA), and then incubated for 10 min on ice in HKM-E1 buffer supplemented with 0.1% BSA and with 70 nM Alexa Fluor 647-labeled anti-GFP Nb [33,55]. After incubation with GFP Nb, coverslips were washed three times with HKM-E1 buffer, fixed in 4% paraformaldehyde, and shifted to room temperature. Coverslips were then permeabilized with PBS containing 0.1% Triton X-100 for 10 min, blocked, stained with anti-Rab34 antibody (Abcam), and processed as described above.

Sample preparation for expansion microscopy—Cells were seeded on 25mm #1.5 coverslips (Electron Microscopy Sciences) and prepared as in Sahabandu *et al.*[35] Briefly, cells were fixed in 4% formaldehyde for 1 h, incubated in 30% acrylamide/4% formaldehyde at 37°C for 16 h, washed 3x 10min in PBS and then cooled on ice water. Pre-cooled gelling solution (20% Acrylamide, 0.04% bis-acrylamide, 7% sodium acrylate. 0.5% APS and 0.5% TEMED) was then added, and polymerization was allowed to proceed for 30 min on ice and 30-60 min at room temperature. 4-mm gel punches were taken using a biopsy punch (Integra Miltex , 33-34-P/25) and then denatured in SDS solution (50 mM Tris pH 9.0, 200 mM SDS, 200 mM NaCl) for 1 h at 90°C. Gel punches were allowed to cool, and SDS solution was washed out with PBS (9x 20 min washes) followed by incubation overnight in PBS at 4°C.

Denatured punches were then blocked in immunofluorescence buffer (1% BSA, 0.05% Tween-20 in PBS) for 2 h and incubated overnight at 4°C with primary antibodies in immunofluorescence buffer (see Key Resources Table). Punches were washed in PBS (6x 10 min), then incubated with secondary antibodies and Hoechst 33258 overnight at 4°C. Finally, stained punches were washed in water (12x 10 min), then expanded overnight in deionized water at 4°C. Gels were transferred to 35mm glass-bottom imaging dishes (Mattek P35G-1.5-14-C), immobilized using low-melt agarose, and imaged as described below. We estimate from the final gel size and the size of expanded nuclei that gels expanded ~4-fold, as previously reported.[35]

Fluorescence microscopy—Coverslips with fixed NIH-3T3 and RPE1 cells were imaged using a Nikon Eclipse Ti-2 widefield microscope equipped with a CMOS camera (Photometrics Prime BSI or Hamamatsu Orca-Fusion), a 60× PlanApo oil objective (NA 1.40; Nikon Instruments), and an LED light source (Lumencor Spectra X or SOLA-V-NIR). Fixed samples were mounted in Fluoromount-G and images acquired at room temperature or 37°C using Nikon Elements software. MDCK cells cultured as 2D monolayers were imaged on an Olympus FV1000 confocal microscope using a 60× UPLSAPO oil objective (NA 1.35) controlled with Fluoview software (Olympus). MDCK cells cultured as 3D cysts were imaged on an Olympus IX83 microscope equipped with a Dragonfly200 spinning disk unit (Andor), a CMOS camera (Andor Zyla 4.2 Plus), a 60× UPLSAPO silicone oil objective

Author Manuscript Author Manuscript Author Manuscript Author Manuscript

(NA 1.30), and Fusion software (Andor). Fixed 2D MDCK cells were mounted in ProLong Diamond (Thermo Fisher) and images were acquired at room temperature.

Live-cell imaging and expansion microscopy imaging were performed on a Nikon Eclipse Ti-2 equipped a with Yokogawa W1 spinning disk unit, CMOS camera (Photometrics Prime BSI), 40× PlanApo silicone oil objective (NA 1.25), and laser combiner (Nikon Instruments LUN-F XL 405/488/561/640). For live-cell imaging, 42,000 cells per well were seeded on a μ-slide 8 well plate (Ibidi 80826), and after 24 h cells were imaged in phenol-red-free DMEM/F-12 medium with 10-1000 ng/ml doxycycline and 0.2% serum at 37°C using Nikon Elements software. A Perfect Focus System was used to maintain focus, and a stage-top incubator (Tokai Hit) was used to maintain temperature and 5% CO_2. This system was used for all live-cell imaging, except for imaging of Ehd1-mScarlet-I, which was performed on the widefield Eclipse Ti-2 used for fixed-cell imaging (using an Okolab enclosure to maintain cells at 37°C and 5% CO_2). For expansion microscopy, samples were imaged at room temperature and the supplemental 1.5x magnification tube lens of the Eclipse Ti-2 was used with the 40× PlanApo silicone oil objective (NA 1.25).

Structured illumination microscopy (SIM) imaging was performed on a Deltavision OMX v3 microscope (Applied Precision) equipped with a U-PLANAPO 60× oil objective (NA 1.42; Olympus), CoolSNAP HQ^2 CCD cameras (Photometrics), and solid-state lasers at 488, 561, and 642 nm (Coherent and MPB communications). Samples were illuminated by a coherent scrambled laser light source that had passed through a diffraction grating to generate the structured illumination by interference of light orders in the image plane to create a 3D sinusoidal pattern, with lateral stripes approximately 270 nm apart. The pattern was shifted laterally through five phases and through three angular rotations of 60° for each z section (separated by 125 nm). Cells were stained with antibodies to Rab34 (Abcam) and ARL13B (NeuroMab), mounted in Prolong Diamond medium (Invitrogen P36965), and imaged at room temperature. Raw images were processed and deconvolved using Softworx software (Applied Precision). Channels acquired on separate cameras were then aligned in x, y, z, and rotationally using the SoftWorx alignment tool and Tetraspeck beads (Invitrogen T7279).

Focused ion beam scanning electron microscopy (FIB-SEM)—Cells cultured on 12mm glass coverslips were fixed in 4% PFA for 20 min, washed in PBS, and further fixed in 2% glutaraldehyde in 0.1 M sodium cacodylate buffer, 2% OsO_4 and 1.5% $K_4Fe(CN)_6$ (Sigma-Aldrich). Fixed cells were then stained en bloc in 2% aqueous uranyl acetate, dehydrated, and embedded in Embed 812. Unless otherwise noted, all FIB-SEM reagents are from Electron Microscopy Sciences.

After removing the glass coverslip, the embedded monolayer of cultured cells was glued with EMS water-based conductive graphene carbon paint onto the sample mounting aluminum stub, with the coverslip-facing side of the cells exposed to the air. A 20-25 nm-thick conductive platinum coating was applied to the sample surface with a sputter coater (Ted Pella, Inc.), and the sample was then imaged in a Crossbeam 550 FIB-SEM workstation (Carl Zeiss Microscopy) operated with SmartSEM (Carl Zeiss Microscopy) or Atlas engine 5 (Fibics Incorporated, Ottawa, Canada) software. For image acquisition, a

Author Manuscript Author Manuscript Author Manuscript Author Manuscript

target area was first selected with the SE2 detector (Electron High Tension], 5kV; electron beam current, 2nA) at working distance of 10 nm, then the stage was inclined (to 54°) and lifted (to a working distance of 5 nm) as the eucentric height and coincident point were adjusted. The targeted cells' surface (50x30 μm) was deposited with a 0.5-1 μm-thick protective platinum pad by using 30kV:3nA FIB. Autotune marks and 3D tracking marks were milled into the platinum pad, and carbon deposited by 30kV:50pA FIB, followed by deposition of another 0.5-1 μm-thick upper protective carbon pad. 30kV:30nA FIB was used for the coarse trench (20 μm deep), 30kV:3nA FIB was used for the fine trench, and 30kV:300pA FIB was used for milling the imaging surface during the 3D tracking. The dwell time for SEM imaging (Electron High Tension, 1.5 kV; electron beam current, 2 nA) with EsB detector was set at 2-3 μs with line averaging by 2. The filtering grid voltage of the EsB detector was set at 1000 V, and the collector voltage was set at 300 *V*. The imaging resolution was set at 7 nm/pixel at X, Y axis, slicing by 7 nm along Z axis, yielding final data sets with isotropic resolution at 7 nm/voxel. After the FIB-SEM imaging, the data sets were aligned and exported with Atlas 5 software, then further cropped and rotated with DragonFly software (Object Research Systems Inc.).

Image analysis—Widefield fluorescence microscopy images were analyzed using Fiji/ImageJ. Ciliogenesis and quantification of protein markers present at cilia or centrioles was performed by manual counting. For SIM microscopy, images that were deconvolved using Softworx software (see above) were further aligned using Tetraspeck bead images and the Fiji Descriptor-based registration (2D) plugin. Intensity values for line traces across SIM images were determined in Fiji/Image using the 'Plot Profile' tool and plotted using Matlab (Mathworks, Inc.).

FIB-SEM datasets were processed using IMOD software.[57,58] Rotated sub-volumes were extracted using the 'Rubber band' tool. Centrioles and associated membranes were segmented using the 'Sculp' drawing tool and rendered with the Surface and Cap Meshing options.

Transfection, immunoprecipitation, SDS-PAGE, and Western blotting—HEK293T cells were transfected with LAP-Rab34 variants using X-tremeGENE 9 (Sigma Aldrich, 6365779001). After 48 h, the cells were collected, lysed on ice in Co-IP buffer (50 mM Tris pH 7.4, 150 mM NaCl, 1% Triton X-100, 0.5 mM DTT, protease inhibitors), and centrifuged at 20,000 x *g* for 15 min. LAP-tagged proteins were captured on GFP nanobody beads (Chromotek #gta-20). After washing, the beads were resuspended in 2X NuPAGE LDS buffer (Invitrogen) and denatured at 95°C for 5 min to elute captured proteins. For analysis of Rab34 levels in whole-cell lysate, cells were lysed in RIPA buffer (50 mM Tris pH 7.4, 150 mM NaCl, 2% NP40, 0.25% sodium deoxycholate, 0.5 mM DTT, protease inhibitors) on ice for 10 min and centrifuged at 20,000 x *g* for 10 min. The supernatant was collected, and equal amounts of protein were loaded, as determined by Bio-Rad Protein Assay.

Protein samples were separated on NuPAGE 4-12% Bis-Tris gels (Invitrogen) run in MOPS buffer (50 mM Tris, 50 mM MOPS, 3.5 mM SDS, 1 mM EDTA) and transferred to a PVDF membrane (Millipore Sigma #IPVH00010). The membranes were blocked in 1:1 PBS/

Author Manuscript Author Manuscript Author Manuscript Author Manuscript

SeaBlock (Thermo Fisher #37527) and incubated with primary antibodies overnight at 4°C (see Key Resources Table). After washing, the membranes were incubated with HRP-conjugated secondary antibodies or Protein A-HRP for 30 min at room temperature. The blots were developed using Clarity Western ECL Substrate (Bio-Rad) and imaged on a ChemiDoc Touch imager (Bio-Rad).

Analysis of GTP/GDP binding in cells—HEK293T cells were transfected with LAP-Rab34 variants using X-tremeGENE 9. After 48 h, the cells were incubated with 0.25 mCi of ^{32}P orthophosphate (Perkin Elmer, NEX053H002MC) for 4 h in DMEM containing dialyzed FBS (Gibco A3382001). The labeled cells were washed with ice-cold PBS and lysed on ice in Co-IP buffer supplemented with 10 mM $MgCl_2$. The lysate was clarified by centrifugation at 20,000 x *g* for 15 min at 4°C, and LAP-tagged proteins were captured on GFP nanobody beads. After washing, bound nucleotides were dissociated by incubation in Elution buffer (0.2% SDS, 4 mM EDTA, 2 mM DTT, 1 mM GDP, 1 mM GTP) for 6 min at 68°C. The eluate was then spotted on a PEI-cellulose TLC plate (Sigma Z122882) and developed in a chamber equilibrated with 0.75 M KH_2PO_4. The dried plate was exposed to a phosphorimaging screen for 24 h, imaged on a Typhoon FLA 9500 (GE Healthcare), and quantified using ImageQuant software (GE Healthcare).

Recombinant protein expression and purification—pGEX-Rab34 plasmids were transformed into BL21 DE3 competent cells expressing GroEL/ES (from pGro7 plasmid; gift from Yong Xiong, Yale University) and selected with 100 μg/mL ampicillin and 25 μg/mL chloramphenicol. Transformed cells were inoculated into a 100 mL culture of LB with ampicillin and chloramphenicol and grown at 37°C for 16 h. This culture was diluted to OD_{600}=0.02-0.06 and expanded to 4L, followed by growth at 37°C until OD_{600}=0.6. The cultures were then cooled in an ice water bath for 15 min. 2g/L arabinose was added to induce pGro7 expression and the cultures were transferred to an 18°C incubator. After 30 min, 200 μM IPTG was added to induce the expression of GST-Rab34. The cultures were grown at 18°C overnight; cultures were then collected by centrifugation, and the cells were flash frozen.

Cell pellets were suspended in lysis buffer (10 mM Tris pH 7.3, 1 mM DTT, 150 mM NaCl, 5 mM $MgCl_2$, 0.001% Triton X-100, 1mM PMSF, 0.2 mM GDP, Roche cOmplete EDTA-free protease inhibitors) and lysed with a microfluidizer. Cell debris was removed through a high-speed (20,000 x *g*) clarification spin. The resulting supernatant was incubated with Glutathione Sepharose resin (GE Healthcare, 17-0756-05) for 2 h in lysis buffer. Bound Rab34 was eluted with elution buffer (10 mM Tris pH 8.2, 10 mM glutathione, 1 mM DTT, 70 mM NaCl, 5 mM $MgCl_2$). Eluted Rab34 was then diluted 1:5 with Buffer A (10 mM Tris pH 8.2, 1 mM DTT, 70 mM NaCl, 5 mM $MgCl_2$), loaded onto an anion exchange column (GE Healthcare HiTrap Q, 17-5156-01), washed with 10 column volumes of Buffer A, and eluted with a linear gradient of 0% to 100% Buffer B (10 mM Tris pH 8.2, 1 mM DTT, 0.5 M NaCl, 5 mM $MgCl_2$) over 20 column volumes. Rab34-containing fractions were dialyzed overnight into storage buffer (50 mM Tris pH 7.5, 1 mM DTT, 150 mM NaCl, 5 mM $MgCl_2$, 0.2 mM GDP) and simultaneously treated with HRV3C Protease (Pierce 88946) to cleave the GST tag. Dialyzed Rab34 was then concentrated to approximately 70 μM with an

Author Manuscript Author Manuscript Author Manuscript Author Manuscript

Amicon concentrator (Millipore, Z740199). Free GST tag, uncleaved GST-Rab34, and HRV3C were removed via a second incubation with Glutathione Sepharose resin. Lastly, glycerol was added to a final concentration of 40% (v/v) and the purified Rab34 was stored at −20°C. All steps were conducted at 4°C unless noted otherwise.

Analysis of GTPase activity in vitro—All Rab34 used in steady-state assays was treated with AG 1-X8 anion exchange resin (Bio-Rad, 1401441) immediately before use to remove bound GDP. Steady-state GTPase activity was measured with a modified version of the standard NADH-based assay[59,60], in which the final concentrations of coupling reaction components were adjusted as follows: pyruvate kinase (Sigma Aldrich, P9136) – 400 units/mL; lactate dehydrogenase (BBI Enzymes, LDHP2FS) – 40 units/mL; phosphoenolpyruvate (Sigma Aldrich, 10108294) – 10 mM. Rab34 GTPase activity was assayed in Rab34 assay buffer (50 mM Tris pH 7.7, 150 mM NaCl, 5 mM $MgCl_2$, 1 mM DTT) at 25°C. Absorbance at 340 nm was measured on an Olis HP 8452 Diode Array spectrophotometer.

QUANTIFICATION AND STATISTICAL ANALYSIS

Statistical analysis—Statistical tests were carried out using t-test (two-sided, paired) or Tukey-Kramer test, as indicated in Figure Legends. Figure legends also indicate the number of independent replicates performed and the number of cells analyzed for each condition of each replicate (*N*). All graphs show the mean and SEM unless otherwise noted.

Supplementary Material

Refer to Web version on PubMed Central for supplementary material.

Acknowledgments

We acknowledge David Mick and members of the D.K.B. lab for advice and discussion; Derek Toomre (Yale University) for the In/Out reporter construct and cell line; Jadranka Loncarek (National Cancer Institute) for advice on expansion microscopy; Chris Westlake (National Cancer Institute) for cDNA encoding EHD1; Tamara Caspary (Emory University) for ARL13B cDNA; Tim Stearns (Stanford University) for Centrin2 cDNA; and Yong Xiong (Yale University) for pGro7 plasmid. This work was supported by funding from the National Institutes of Health (R00HD082280 and R35GM137956 to D.K.B.; R35GM136656 to E.M.D.L.C.), the Charles H. Hood Foundation (to D.K.B.), the Alfred P. Sloan Foundation (FG-2018-10333 to D.K.B.), a Yale Anderson Endowed Fellowship (A.K.G.), the Ministry of Education, Culture, Sports, Science and Technology (MEXT) of Japan (Grant-in-Aid for Young Scientists 20K15739 to Y.H.; Grant-in-Aid for Scientific Research(B) 19H03220 to M.F.), the Japan Science and Technology Agency (CREST grant JPMJCR17H4 to M.F.), the Japan Society for the Promotion of Science (to M.E.O.), and NSF major instrumentation grant 1725480. S.D.G. was supported by R35GM136656-S1. We acknowledge Felix Rivera-Molina, Derek Toomre, and the Yale CINEMA microscopy facility for assistance with SIM imaging; Yumei Wu, Xinran Liu, and the Yale Center for Cellular and Molecular Imaging for FIB-SEM sample processing and data collection; Ken Nelson and the MCDB FACS facility for assistance with cell sorting; Shirin Bahmanyar, Jing Yan, and Nadya Dimitrova for microscope use; Anna Pyle for phosphorimager use; Brandon Toyama for graphical assistance; and Kazuyasu Shoji for assistance with Western blotting.

References

1. Braun DA, and Hildebrandt F (2017). Ciliopathies. Cold Spring Harb Perspect Biol 9, a028191. 10.1101/cshperspect.a028191. [PubMed: 27793968]
2. Anvarian Z, Mykytyn K, Mukhopadhyay S, Pedersen LB, and Christensen ST (2019). Cellular signalling by primary cilia in development, organ function and disease. Nat Rev Nephrol 15, 199–219. 10.1038/s41581-019-0116-9. [PubMed: 30733609]

Author Manuscript Author Manuscript Author Manuscript Author Manuscript

3. Reiter JF, and Leroux MR (2017). Genes and molecular pathways underpinning ciliopathies. Nat Rev Mol Cell Biol 18, 533–547. 10.1038/nrm.2017.60. [PubMed: 28698599]
4. Sorokin S (1962). Centrioles and the formation of rudimentary cilia by fibroblasts and smooth muscle cells. J Cell Biol 15, 363–377. 10.1083/jcb.15.2.363. [PubMed: 13978319]
5. Sorokin SP (1968). Reconstructions of centriole formation and ciliogenesis in mammalian lungs. J Cell Sci 3, 207–230. [PubMed: 5661997]
6. Insinna C, Lu Q, Teixeira I, Harned A, Semler EM, Stauffer J, Magidson V, Tiwari A, Kenworthy AK, Narayan K, and Westlake CJ (2019). Investigation of F-BAR domain PACSIN proteins uncovers membrane tubulation function in cilia assembly and transport. Nat Commun 10, 428. 10.1038/s41467-018-08192-9. [PubMed: 30683896]
7. Lu Q, Insinna C, Ott C, Stauffer J, Pintado PA, Rahajeng J, Baxa U, Walia V, Cuenca A, Hwang YS, et al. (2015). Early steps in primary cilium assembly require EHD1/EHD3-dependent ciliary vesicle formation. Nat Cell Biol 17, 228–240. 10.1038/ncb3109. [PubMed: 25686250]
8. Wu CT, Chen HY, and Tang TK (2018). Myosin-Va is required for preciliary vesicle transportation to the mother centriole during ciliogenesis. Nat Cell Biol 20, 175–185. 10.1038/s41556-017-0018-7. [PubMed: 29335527]
9. Mazo G, Soplop N, Wang WJ, Uryu K, and Tsou MF (2016). Spatial Control of Primary Ciliogenesis by Subdistal Appendages Alters Sensation-Associated Properties of Cilia. Dev Cell 39, 424–437. 10.1016/j.devcel.2016.10.006. [PubMed: 27818179]
10. Ghossoub R, Molla-Herman A, Bastin P, and Benmerah A (2011). The ciliary pocket:a once-forgotten membrane domain at the base of cilia. Biol Cell 103, 131–144. 10.1042/BC20100128. [PubMed: 21275905]
11. Pusapati GV, Kong JH, Patel BB, Krishnan A, Sagner A, Kinnebrew M, Briscoe J, Aravind L, and Rohatgi R (2018). CRISPR Screens Uncover Genes that Regulate Target Cell Sensitivity to the Morphogen Sonic Hedgehog. Dev Cell 44, 113–129 e8. 10.1016/j.devcel.2017.12.003. [PubMed: 29290584]
12. Xu S, Liu Y, Meng Q, and Wang B (2018). Rab34 small GTPase is required for Hedgehog signaling and an early step of ciliary vesicle formation in mouse. J Cell Sci 131, jcs213710. 10.1242/jcs.213710. [PubMed: 30301781]
13. Oguchi ME, Okuyama K, Homma Y, and Fukuda M (2020). A comprehensive analysis of Rab GTPases reveals a role for Rab34 in serum starvation-induced primary ciliogenesis. J Biol Chem 295, 12674–12685. 10.1074/jbc.RA119.012233. [PubMed: 32669361]
14. Breslow DK, Hoogendoorn S, Kopp AR, Morgens DW, Vu BK, Kennedy MC, Han K, Li A, Hess GT, Bassik MC, et al. (2018). A CRISPR-based screen for Hedgehog signaling provides insights into ciliary function and ciliopathies. Nat Genet 50, 460–471. 10.1038/s41588-018-0054-7. [PubMed: 29459677]
15. Pfeffer SR (2017). Rab GTPases: master regulators that establish the secretory and endocytic pathways. Mol Biol Cell 28, 712–715. 10.1091/mbc.E16-10-0737. [PubMed: 28292916]
16. Wandinger-Ness A, and Zerial M (2014). Rab proteins and the compartmentalization of the endosomal system. Cold Spring Harb Perspect Biol 6, a022616. 10.1101/cshperspect.a022616. [PubMed: 25341920]
17. Stenmark H (2009). Rab GTPases as coordinators of vesicle traffic. Nat Rev Mol Cell Biol 10, 513–525. 10.1038/nrm2728. [PubMed: 19603039]
18. Muller MP, and Goody RS (2018). Molecular control of Rab activity by GEFs, GAPs and GDI. Small GTPases 9, 5–21. 10.1080/21541248.2016.1276999. [PubMed: 28055292]
19. Lee MT, Mishra A, and Lambright DG (2009). Structural mechanisms for regulation of membrane traffic by rab GTPases. Traffic 10, 1377–1389. 10.1111/j.1600-0854.2009.00942.x. [PubMed: 19522756]
20. Prior IA, Lewis PD, and Mattos C (2012). A comprehensive survey of Ras mutations in cancer. Cancer Res 72, 2457–2467. 10.1158/0008-5472.CAN-11-2612. [PubMed: 22589270]
21. Tisdale EJ, Bourne JR, Khosravi-Far R, Der CJ, and Balch WE (1992). GTP-binding mutants of rab1 and rab2 are potent inhibitors of vesicular transport from the endoplasmic reticulum to the Golgi complex. J Cell Biol 119, 749–761. 10.1083/jcb.119.4.749. [PubMed: 1429835]

Author Manuscript Author Manuscript Author Manuscript Author Manuscript

22. Walworth NC, Goud B, Kabcenell AK, and Novick PJ (1989). Mutational analysis of SEC4 suggests a cyclical mechanism for the regulation of vesicular traffic. EMBO J 8, 1685–1693. [PubMed: 2504585]

23. Sun P, Yamamoto H, Suetsugu S, Miki H, Takenawa T, and Endo T (2003). Small GTPase Rah/Rab34 is associated with membrane ruffles and macropinosomes and promotes macropinosome formation. J Biol Chem 278, 4063–4071. 10.1074/jbc.M208699200. [PubMed: 12446704]

24. Langemeyer L, Nunes Bastos R, Cai Y, Itzen A, Reinisch KM, and Barr FA (2014). Diversity and plasticity in Rab GTPase nucleotide release mechanism has consequences for Rab activation and inactivation. Elife 3, e01623. 10.7554/eLife.01623. [PubMed: 24520163]

25. Fukuda M, Kanno E, Ishibashi K, and Itoh T (2008). Large scale screening for novel rab effectors reveals unexpected broad Rab binding specificity. Mol Cell Proteomics 7, 1031–1042. 10.1074/mcp.M700569-MCP200. [PubMed: 18256213]

26. Matsui T, Ohbayashi N, and Fukuda M (2012). The Rab interacting lysosomal protein (RILP) homology domain functions as a novel effector domain for small GTPase Rab36:Rab36 regulates retrograde melanosome transport in melanocytes. J Biol Chem 287, 28619–28631. 10.1074/jbc.M112.370544. [PubMed: 22740695]

27. Schmidt KN, Kuhns S, Neuner A, Hub B, Zentgraf H, and Pereira G (2012). Cep164 mediates vesicular docking to the mother centriole during early steps of ciliogenesis. J Cell Biol 199, 1083–1101. 10.1083/jcb.201202126. [PubMed: 23253480]

28. Bernabe-Rubio M, and Alonso MA (2017). Routes and machinery of primary cilium biogenesis. Cell Mol Life Sci 74, 4077–4095. 10.1007/s00018-017-2570-5. [PubMed: 28624967]

29. Nachury MV, and Mick DU (2019). Establishing and regulating the composition of cilia for signal transduction. Nat Rev Mol Cell Biol 20, 389–405. 10.1038/s41580-019-0116-4. [PubMed: 30948801]

30. Breslow DK, and Holland AJ (2019). Mechanism and Regulation of Centriole and Cilium Biogenesis. Annu Rev Biochem 88, 691–724. 10.1146/annurev-biochem-013118-111153. [PubMed: 30601682]

31. Mirvis M, Stearns T, and James Nelson W (2018). Cilium structure, assembly, and disassembly regulated by the cytoskeleton. Biochem J 475, 2329–2353. 10.1042/BCJ20170453. [PubMed: 30064990]

32. Kukic I, Rivera-Molina F, and Toomre D (2016). The IN/OUT assay: a new tool to study ciliogenesis. Cilia 5, 23. 10.1186/s13630-016-0044-2. [PubMed: 27493724]

33. Kirchhofer A, Helma J, Schmidthals K, Frauer C, Cui S, Karcher A, Pellis M, Muyldermans S, Casas-Delucchi CS, Cardoso MC, et al. (2010). Modulation of protein properties in living cells using nanobodies. Nat Struct Mol Biol 17, 133–138. 10.1038/nsmb.1727. [PubMed: 20010839]

34. Tillberg PW, and Chen F (2019). Expansion Microscopy: Scalable and Convenient Super-Resolution Microscopy. Annu Rev Cell Dev Biol 35, 683–701. 10.1146/annurev-cellbio-100818-125320. [PubMed: 31424964]

35. Sahabandu N, Kong D, Magidson V, Nanjundappa R, Sullenberger C, Mahjoub MR, and Loncarek J (2019). Expansion microscopy for the analysis of centrioles and cilia. J Microsc 276, 145–159. 10.1111/jmi.12841. [PubMed: 31691972]

36. Bernabe-Rubio M, Andres G, Casares-Arias J, Fernandez-Barrera J, Rangel L, Reglero-Real N, Gershlick DC, Fernandez JJ, Millan J, Correas I, et al. (2016). Novel role for the midbody in primary ciliogenesis by polarized epithelial cells. J Cell Biol 214, 259–273. 10.1083/jcb.201601020. [PubMed: 27458130]

37. Jewett CE, Soh AWJ, Lin CH, Lu Q, Lencer E, Westlake CJ, Pearson CG, and Prekeris R (2021). RAB19 Directs Cortical Remodeling and Membrane Growth for Primary Ciliogenesis. Dev Cell 56, 325–340 e8. 10.1016/j.devcel.2020.12.003. [PubMed: 33561422]

38. Homma Y, Kinoshita R, Kuchitsu Y, Wawro PS, Marubashi S, Oguchi ME, Ishida M, Fujita N, and Fukuda M (2019). Comprehensive knockout analysis of the Rab family GTPases in epithelial cells. J Cell Biol 218, 2035–2050. 10.1083/jcb.201810134. [PubMed: 31072826]

39. Kohli P, Hohne M, Jungst C, Bertsch S, Ebert LK, Schauss AC, Benzing T, Rinschen MM, and Schermer B (2017). The ciliary membrane-associated proteome reveals actin-binding proteins as

Author Manuscript Author Manuscript Author Manuscript Author Manuscript

key components of cilia. EMBO Rep 18, 1521–1535. 10.15252/embr.201643846. [PubMed: 28710093]

40. Mercer JA, Seperack PK, Strobel MC, Copeland NG, and Jenkins NA (1991). Novel myosin heavy chain encoded by murine *dilute* coat colour locus. Nature 349, 709–713. 10.1038/349709a0. [PubMed: 1996138]
41. Bhattacharyya S, Rainey MA, Arya P, Mohapatra BC, Mushtaq I, Dutta S, George M, Storck MD, McComb RD, Muirhead D, et al. (2016). Endocytic recycling protein EHD1 regulates primary cilia morphogenesis and SHH signaling during neural tube development. Sci Rep 6, 20727. 10.1038/srep20727. [PubMed: 26884322]
42. Rapaport D, Auerbach W, Naslavsky N, Pasmanik-Chor M, Galperin E, Fein A, Caplan S, Joyner AL, and Horowitz M (2006). Recycling to the plasma membrane is delayed in EHD1 knockout mice. Traffic 7, 52–60. 10.1111/j.1600-0854.2005.00359.x. [PubMed: 16445686]
43. Rainey MA, George M, Ying G, Akakura R, Burgess DJ, Siefker E, Bargar T, Doglio L, Crawford SE, Todd GL, et al. (2010). The endocytic recycling regulator EHD1 is essential for spermatogenesis and male fertility in mice. BMC Dev Biol 10, 37. 10.1186/1471-213X-10-37. [PubMed: 20359371]
44. Diekmann Y, Seixas E, Gouw M, Tavares-Cadete F, Seabra MC, and Pereira-Leal JB (2011). Thousands of Rab GTPases for the cell biologist. PLoS Comput Biol 7, e1002217. 10.1371/journal.pcbi.1002217. [PubMed: 22022256]
45. Dickinson ME, Flenniken AM, Ji X, Teboul L, Wong MD, White JK, Meehan TF, Weninger WJ, Westerberg H, Adissu H, et al. (2016). High-throughput discovery of novel developmental phenotypes. Nature 537, 508–514. 10.1038/nature19356. [PubMed: 27626380]
46. Huangfu D, Liu A, Rakeman AS, Murcia NS, Niswander L, and Anderson KV (2003). Hedgehog signalling in the mouse requires intraflagellar transport proteins. Nature 426, 83–87. 10.1038/nature02061. [PubMed: 14603322]
47. Liem KF Jr., Ashe A, He M, Satir P, Moran J, Beier D, Wicking C, and Anderson KV (2012). The IFT-A complex regulates Shh signaling through cilia structure and membrane protein trafficking. J Cell Biol 197, 789–800. 10.1083/jcb.201110049. [PubMed: 22689656]
48. He M, Subramanian R, Bangs F, Omelchenko T, Liem KF Jr., Kapoor TM, and Anderson KV (2014). The kinesin-4 protein Kif7 regulates mammalian Hedgehog signalling by organizing the cilium tip compartment. Nat Cell Biol 16, 663–672. 10.1038/ncb2988. [PubMed: 24952464]
49. Goetz SC, Liem KF Jr., and Anderson KV (2012). The spinocerebellar ataxia-associated gene Tau tubulin kinase 2 controls the initiation of ciliogenesis. Cell 151, 847–858. 10.1016/j.cell.2012.10.010. [PubMed: 23141541]
50. Fonte VG, Searls RL, Hilfer SR The relationship of cilia with cell division and differentiation J. Cell Biol, 49 (1971), pp. 226–229. [PubMed: 5555577]
51. Aguilar A, Meunier A, Strehl L, Martinovic J, Bonniere M, Attie-Bitach T, Encha-Razavi F, and Spassky N (2012). Analysis of human samples reveals impaired SHH-dependent cerebellar development in Joubert syndrome/Meckel syndrome. Proc Natl Acad Sci U S A 109, 16951–16956. 10.1073/pnas.1201408109. [PubMed: 23027964]
52. Vokes SA, Ji H, McCuine S, Tenzen T, Giles S, Zhong S, Longabaugh WJ, Davidson EH, Wong WH, and McMahon AP (2007). Genomic characterization of Gli-activator targets in sonic hedgehog-mediated neural patterning. Development 134, 1977–1989. 10.1242/dev.001966. [PubMed: 17442700]
53. Lee EY, Ji H, Ouyang Z, Zhou B, Ma W, Vokes SA, McMahon AP, Wong WH, and Scott MP (2010). Hedgehog pathway-regulated gene networks in cerebellum development and tumorigenesis. Proc Natl Acad Sci U S A 107, 9736–9741. 10.1073/pnas.1004602107. [PubMed: 20460306]
54. Chang CH, Zanini M, Shirvani H, Cheng JS, Yu H, Feng CH, Mercier AL, Hung SY, Forget A, Wang CH, et al. (2019). Atoh1 Controls Primary Cilia Formation to Allow for SHH-Triggered Granule Neuron Progenitor Proliferation. Dev Cell 48, 184–199 e5.10.1016/j.devcel.2018.12.017. [PubMed: 30695697]

Author Manuscript Author Manuscript Author Manuscript Author Manuscript

55. Breslow DK, Koslover EF, Seydel F, Spakowitz AJ, and Nachury MV (2013). An in vitro assay for entry into cilia reveals unique properties of the soluble diffusion barrier. J Cell Biol 203, 129–147. 10.1083/jcb.201212024. [PubMed: 24100294]

56. Ye F, Breslow DK, Koslover EF, Spakowitz AJ, Nelson WJ, and Nachury MV (2013). Single molecule imaging reveals a major role for diffusion in the exploration of ciliary space by signaling receptors. Elife 2, e00654. 10.7554/eLife.00654. [PubMed: 23930224]

57. Mastronarde DN, and Held SR (2017). Automated tilt series alignment and tomographic reconstruction in IMOD. J Struct Biol 197, 102–113. 10.1016/j.jsb.2016.07.011. [PubMed: 27444392]

58. Kremer JR, Mastronarde DN, and McIntosh JR (1996). Computer visualization of three-dimensional image data using IMOD. J Struct Biol 116, 71–76. 10.1006/jsbi.1996.0013. [PubMed: 8742726]

59. Ingerman E, and Nunnari J (2005). A continuous, regenerative coupled GTPase assay for dynamin-related proteins. Methods Enzymol 404, 611–619. 10.1016/S0076-6879(05)04053-X. [PubMed: 16413304]

60. Bradley MJ, and De La Cruz EM (2012). Analyzing ATP utilization by DEAD-Box RNA helicases using kinetic and equilibrium methods. Methods Enzymol 511, 29–63. 10.1016/B978-0-12-396546-2.00002-4. [PubMed: 22713314]

Author Manuscript Author Manuscript Author Manuscript Author Manuscript

Highlights:

- Rab34 is required for ciliary vesicle formation during ciliogenesis
- Rab34 localizes to nascent ciliary membranes and marks the ciliary sheath
- GTP binding and hydrolysis by Rab34 are required for intracellular ciliogenesis
- Rab34 is dispensable for the extracellular ciliogenesis pathway used by MDCK cells

Author Manuscript Author Manuscript Author Manuscript Author Manuscript

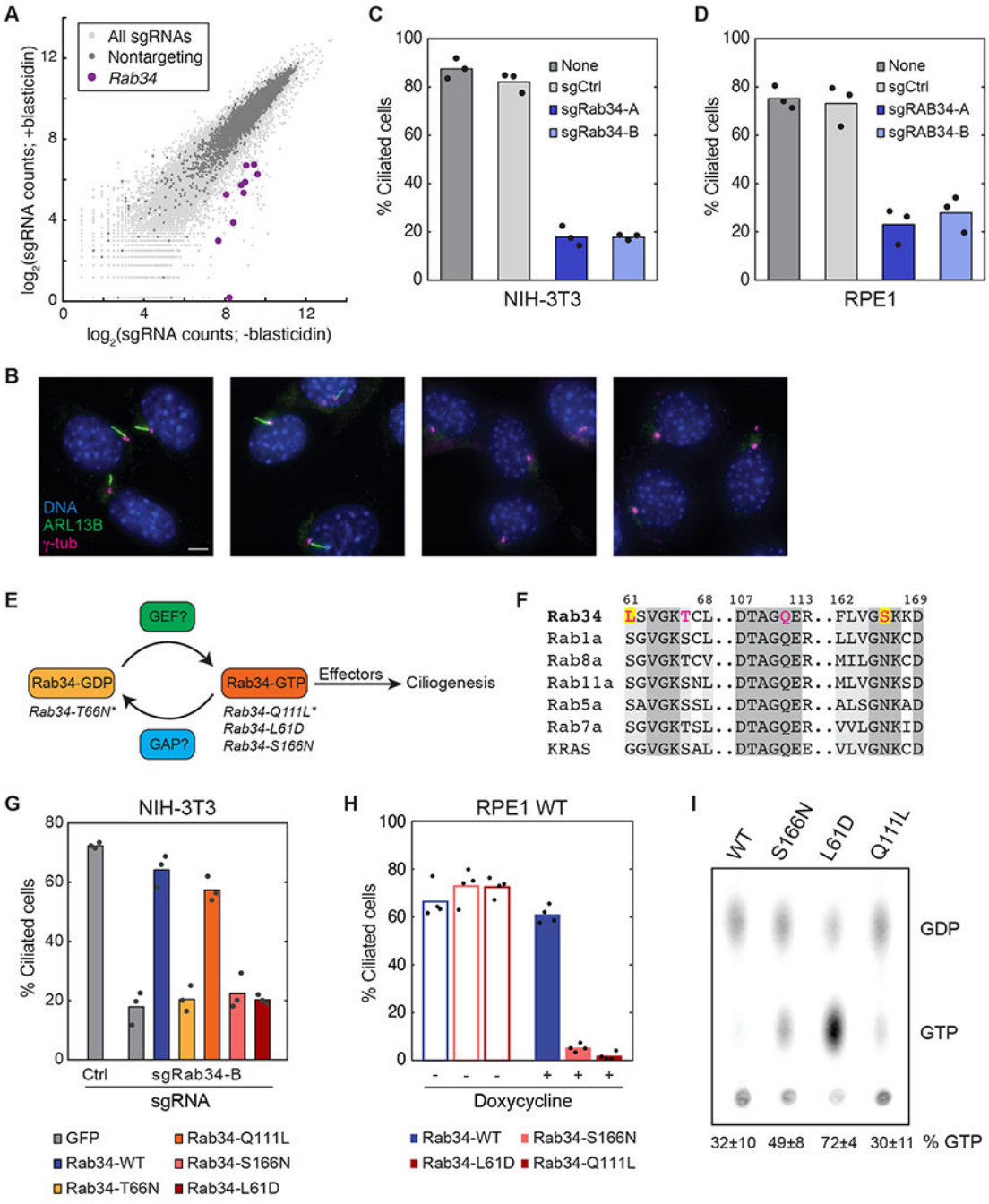

Figure 1. The nucleotide cycle of atypical GTPase Rab34 is required for ciliogenesis in NIH-3T3 and RPE1 cells.

A) Results of a genome-wide CRISPR screen for Hedgehog (Hh) signaling[14] in which signaling-deficient mutants become hypersensitive to blasticidin. The sgRNAs targeting *Rab34* are highlighted. **B**) Cilia (marked by ARL13B) and centrioles (marked by γ-tubulin) were stained in NIH-3T3 cells transduced with the indicated sgRNAs following 24 h serum starvation. Scale bar: 5 μm. **C**) Quantification of ciliogenesis in NIH-3T3 cells shown in (**B**); bars indicate means and dots show values from >120 cells analyzed in each of *N*=3

Author Manuscript Author Manuscript Author Manuscript Author Manuscript

independent experiments. **D**) Quantification of ciliogenesis in RPE1 cells transduced with the indicated sgRNAs and stained as in (**B**) following 48 h serum starvation; bars indicate means and dots show values from >130 cells analyzed in each of *N*=3 independent experiments. See also Figure S1C. E) Illustration of the Rab34 nucleotide cycle including Guanine nucleotide Exchange Factors (GEFs), GTPase Activating Proteins (GAPs), and effectors that support its role in ciliogenesis. Mutants of interest and their nucleotide state are shown (predicted nucleotide states are denoted with asterisks; see also panel **I** for observed nucleotide states). **F**) Alignment of key regions of human Rab34 with other human Rab GTPases and KRAS. Conserved residues T66 and Q111 and divergent residues L61 and S166 are indicated. **G**) NIH-3T3 cells transduced with the indicated sgRNAs were transfected with GFP-FKBP or the indicated GFP-Rab34 constructs. Ciliogenesis was assessed as in **C**; bars indicate means and dots show values from >40 cells analyzed in each of *N*=3 independent experiments. **H**) Ciliogenesis was assessed in RPE1 stable cell lines expressing the indicated GFP-Rab34 variants under control of a doxycycline-inducible promoter. Where indicated, doxycycline was included for 24 h preceding serum starvation and during serum starvation. Bars indicate means and dots show values from *N*=4 independent experiments. **I**) Analysis of GTP and GDP bound to GFP-Rab34 following metabolic labeling in HEK-293T cells, anti-GFP immunoprecipitation, thin layer chromatography of bound nucleotides, and autoradiography. Values shown represent mean ± s.e.m. from *N*=3 independent experiments. See also Figure S1.

Author Manuscript Author Manuscript Author Manuscript Author Manuscript

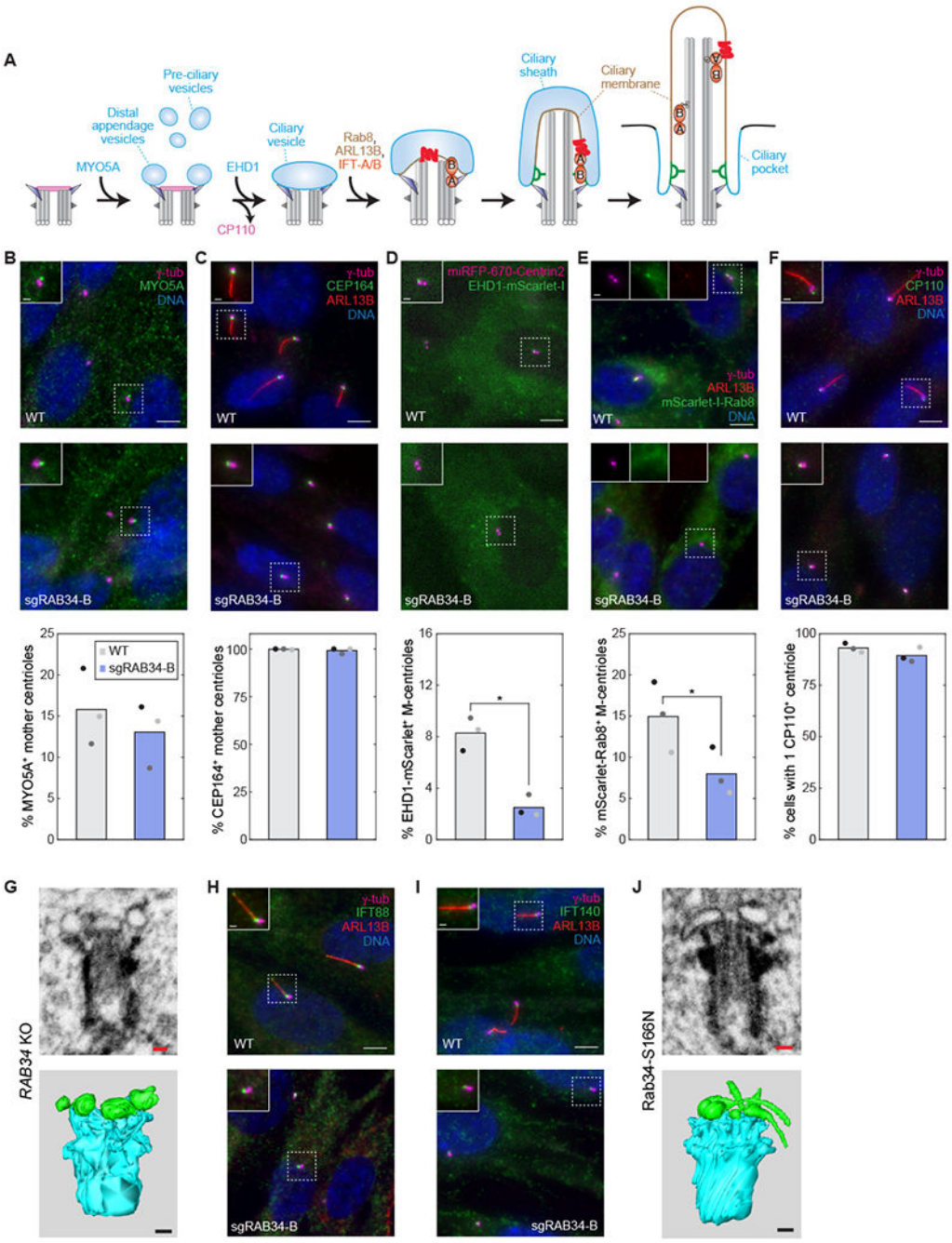

Figure 2. Rab34 is required for formation of the ciliary vesicle from distal appendage vesicles

A) Schematic illustration of the intracellular ciliogenesis pathway, highlighting the stepwise formation of a ciliary vesicle associated with the mother centriole's distal appendages, the growth of this membrane and the axonemal microtubules to yield a nascent intracellular cilium, and the subsequent fusion of the ciliary sheath with the plasma membrane that exposes the cilium to the external environment. IFT-complexes are indicated in orange and a ciliary membrane protein in red. **B-F**) The indicated markers were examined in RPE1 WT and *RAB34* sgRNA-B cells. Distal appendage protein CEP164 and pre-ciliary vesicle

Author Manuscript Author Manuscript Author Manuscript Author Manuscript

trafficking motor MYO5A were immunostained after 48 h and 2 h serum starvation, respectively. Cells stably expressing EHD1-mScarlet-I and miRFP-670-Centrin2 were imaged live 4 h after serum starvation, and cells expressing mScarlet-I-Rab8, marking assembling cilia, were stained 24 h after serum starvation. For dynamic recruitment of MYO5A, EHD1 and Rab8, timepoints were chosen to match when these events occur during ciliogenesis; otherwise, cells were analyzed 48 h after serum starvation when mature cilia have formed. At bottom, the percentage of cells exhibiting localization of the indicated makers to the mother centriole (M-centriole) or cilium (nascent or mature) is shown. Bars indicate means and dots show values from N=3 independent experiments. P-values determined by two-sided paired t-test are $8.18x10^{-3}$ and $2.19x10^{-2}$ for EHD1 and Rab8, respectively; all other comparisons were not significant ($P > 0.1$). Scale bars: 5 μm (insets: 1 μm). **G**) Volumetric analysis of centrioles and associated membranes by focused ion beam scanning electron microscopy (FIB-SEM) was conducted in *RAB34* knockout RPE1 cells (sgRAB34-B pool). 7x7x7nm voxels were acquired and individual slices as well as 3D reconstructions are shown (centrioles are segmented in cyan and vesicles in green). Scale bars: 100 nm. See also Figure S2C. H–I) IFT-B component IFT88 and IFT-A component IFT140 were examined after 48 h serum starvation in RPE1 WT and *RAB34* sgRNA-B cells. Scale bars: 5 μm (insets: 1 μm). **J**) Volumetric analysis of centrioles and associated membranes by FIB-SEM was conducted as in (**G)** for doxycycline-induced RPE1 cells expressing GFP-Rab34-S166N. Scale bars: 100 nm. See also Figure S2.

Author Manuscript Author Manuscript Author Manuscript Author Manuscript

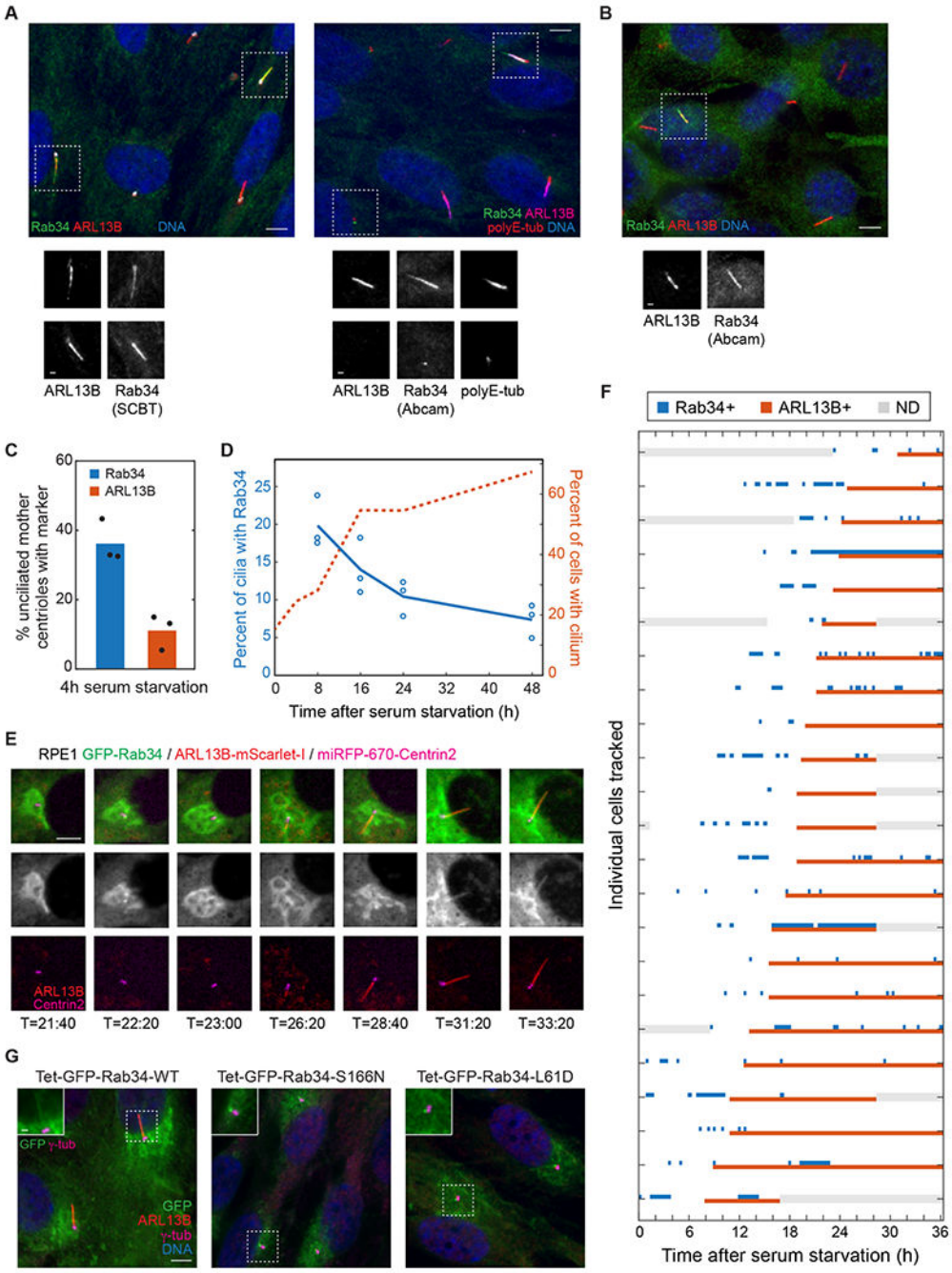

Figure 3. Rab34 dynamically localizes to the mother centriole and cilium during ciliogenesis.

A) RPE1 cells were stained for the indicated ciliary and centriolar markers as well as for Rab34 using antibodies from Santa Cruz Biotechnology (SCBT) or Abcam. Scale bars: 5 μm (insets: 1 μm). **B**) NIH-3T3 cells were stained with the indicated antibodies as in (**A**). **C**) The percent of unciliated centrioles that have recruited puncta of Rab34 or ARL13B was determined 4 h after serum starvation. Bars indicate means and dots show values from each of *N*=3 independent experiments. **D**) The percentage of cilia (marked by ARL13B) that are positive for Rab34 is shown for the indicated times after serum starvation (left-hand Y-axis;

Author Manuscript Author Manuscript Author Manuscript Author Manuscript

the earliest timepoints are omitted due to the low level of ciliation). The percentage of cells with ARL13B-marked cilia is plotted on the right-hand Y-axis. Circles indicate values from individual experiments, and lines show mean from *N*=3 independent experiments. **E**) Time-lapse imaging of RPE1 cell line expressing GFP-Rab34, ARL13B-mScarlet-I, and miRFP-670-Centrin2 was performed, and select images of a representative cell are shown at the indicated times after serum starvation. Scale bar: 5 μm. **F**) Localization of GFP-Rab34 and ARL13B-mScarlet-I was assessed for 23 ciliating cells tracked for up to 36 h after serum starvation. Timepoints when GFP-Rab34 or ARL13B-mScarlet-I were detected at the mother centriole or cilium are indicated by blue and red boxes, respectively; gray boxes indicate when localization could not be determined (ND, e.g. due to cell leaving field of view). Cells are sorted by time of ARL13B arrival and cilium extension. **G**) Localization of GFP-tagged Rab34 was assessed in RPE1 cells stably expressing wildtype Rab34 or the indicated variants. Doxycycline was added prior to and during 48 h serum starvation. Scale bar: 5 μm (inset: 1 μm). See also Figure S3.

Author Manuscript Author Manuscript Author Manuscript Author Manuscript

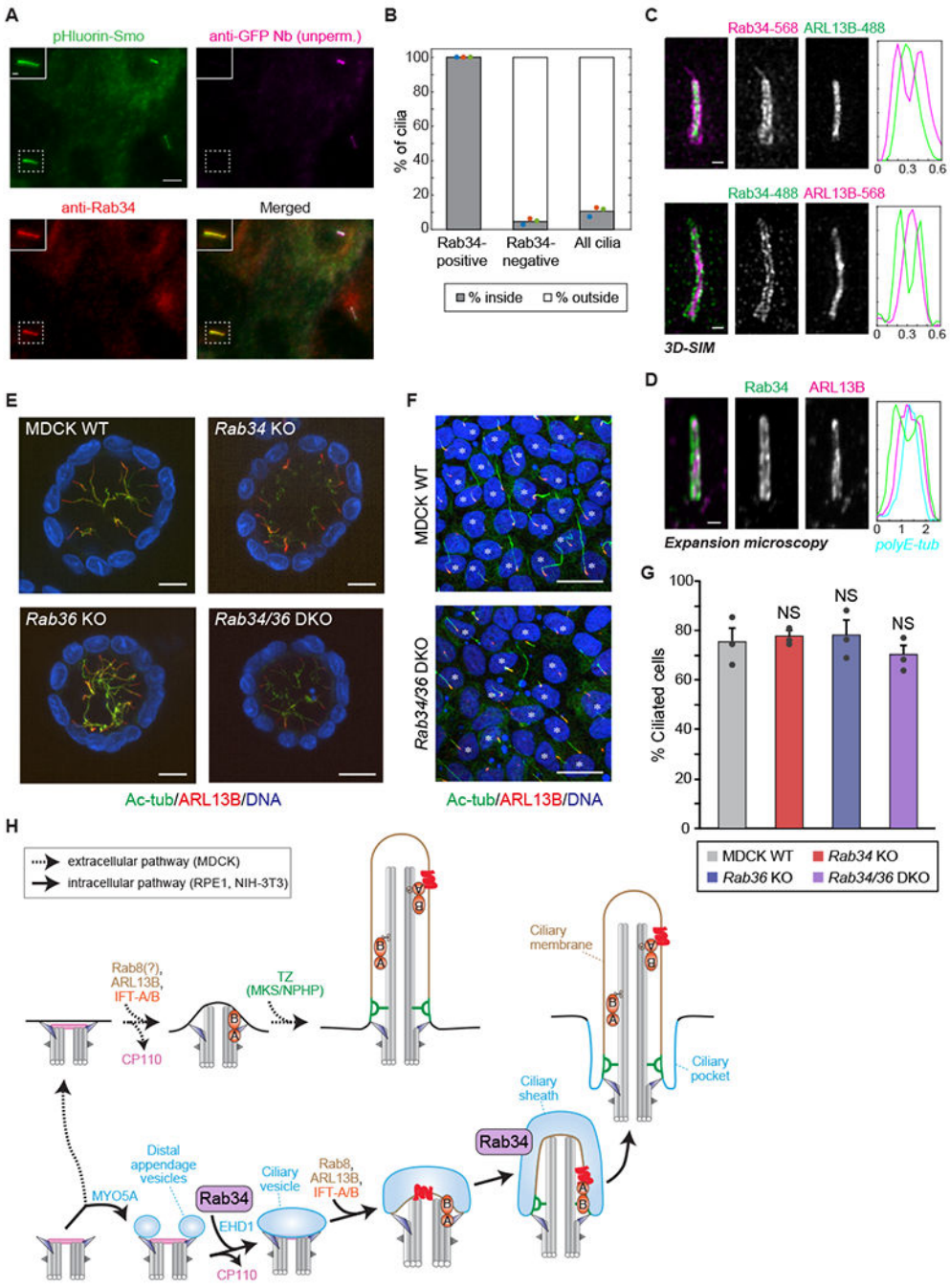

Figure 4. Rab34 localizes to the ciliary sheath of intracellular cilia and is dispensable for extracellular ciliogenesis in MDCK cells

A) RPE1 cells expressing the pHluorin-Smo In/Out reporter were stained prior to permeabilization with anti-GFP nanobody (Nb) to reveal intracellular versus extracellular cilia followed by permeabilization and staining for Rab34 (Abcam antibody). Inset shows an intracellular (inside) cilium that is positive for Rab34. Scale bar: 5 μm (inset: 1 μm). **B**) Quantification of the fraction of cilia that are inside versus outside is shown for the cilia classes indicated. Dots indicate values from individual experiments, and bars indicate means

Author Manuscript Author Manuscript Author Manuscript Author Manuscript

from *N*=3 independent experiments encompassing 110 Rab34-positive cilia and 1,651 Rab34-negative cilia. See also Figure S3C. **C**) 3D-SIM (structured illumination microscopy) was performed on RPE1 cells stained for Rab34 and ARL13B. Graphs at right show normalized fluorescence intensity along line-profiles perpendicular to the longitudinal axis of the cilium. Scale bars: 100 nm. See also Figure S3F. **D**) Expansion microscopy of cells stained for Rab34 and ARL13B. Graph at right shows normalized fluorescence intensity along line-profile across the cilium, including for axonemal polyE-tubulin. Scale bar: 2 μm (after ~4-fold expansion). See also Figure S3G. **E**) Representative images of 3D cysts of parental, *Rab34* knockout (KO), *Rab36* KO, and *Rab34/36* double-knockout (DKO) MDCK cells. The cells were fixed after 7-day culture in collagen gel and then stained for acetylated tubulin (Ac-tub; green), ARL13B (red), and DAPI (blue). Scale bars: 10 μm. **F**) Representative images of 2D monolayers of parental and *Rab34/36* DKO MDCK cells. The cells were fixed 5 days after seeding and then stained as in (**E**). Scale bars: 10 μm. Asterisks indicate ciliated cells. **G**) The percentage of ciliated cells in 2D monolayers of parental, *Rab34* KO, *Rab36* KO, and *Rab34/36* DKO MDCK cells is shown. Dots indicate values from individual experiments, bars indicate means from *N*=3 independent experiments, and error bars indicate standard error. Differences that are not significantly different are marked "NS" (Tukey-Kramer test; $P > 0.60$). **H**) Model for Rab34 function, in which it mediates ciliary membrane formation in the intracellular ciliogenesis pathway (bottom, solid arrows) but not the extracellular ciliogenesis pathway (top, dashed arrows). Rab34 is present on DAVs and the ciliary sheath (blue) but not the ciliary membrane (tan). See also Figures S3 and S4.

Author Manuscript Author Manuscript Author Manuscript Author Manuscript

KEY RESOURCES TABLE

REAGENT or RESOURCE	SOURCE	IDENTIFIER
Antibodies		
Mouse anti-ARL13B	Antibodies Inc. / NeuroMab	Cat#75-287; RRID: AB_2341543
Rabbit anti-ARL13B	Proteintech	Cat#17711-1-AP; RRID: AB_2060867
Rabbit anti-CP110	Proteintech	Cat#12780-1-AP; RRID: AB_10638480
Rabbit anti-CEP164	Sigma Aldrich	Cat#HPA037606; RRID: AB_10672498
Rabbit anti-GDI2	Proteintech	Cat#10116-1-AP: RRID: AB_2279073
Chicken anti-GFP	Invitrogen	Cat#A10262; RRID: AB_2534023
Rabbit anti-GFP	Invitrogen	Cat#A11122; RRID: AB_221569
Rabbit anti-IFT88	Proteintech	Cat#13967-1-AP; RRID: AB_2121979
Rabbit anti-IFT140	Proteintech	Cat#17460-1-AP; RRID: AB_2295648
Rabbit anti-MYO5A	Cell Signaling Technology	Cat#3402; RRID: AB_2148475
Rabbit anti-Rab34	Abcam	Cat#ab73383; RRID: AB_1952423
Mouse anti-Rab34	Santa Cruz Biotechnology	Cat#sc-376710; RRID: AB_11150504
Rabbit anti-Rab34	Proteintech	Cat#27435-1-AP; RRID: AB_2880870
Rabbit anti-Rab34	Fukuda lab[13]	N/A
Rabbit anti-Rab36	Fukuda lab[26]	N/A
Rabbit anti-RILPL1	Sigma Aldrich	Cat#HPA041314; RRID: AB_10795587
Mouse anti-acetylated tubulin	Sigma Aldrich	Cat#T6793; RRID: AB_477585
Mouse anti-gamma tubulin	Sigma Aldrich	Cat#T5326; RRID: AB_532292
Mouse anti-glutamylated tubulin	Adipogen	Cat#AG-20B-0020; RRID: AB_2490210
Donkey anti-Rabbit (Alexa Fluor 488, Cy3, Cy5)	Jackson Immunoresearch	Cat#711-[165/545/605]-152
Goat anti-Mouse IgG1 (Alexa Fluor 488, Cy3, Cy5)	Jackson Immunoresearch	Cat#115-[165/545/605]-205
Goat anti-Mouse IgG2a (Alexa Fluor 488, Cy3, Cy5)	Jackson Immunoresearch	Cat#115-[165/545/605]-206
Goat anti-Mouse IgG2b-Cy3	Jackson Immunoresearch	Cat#115-165-207
Donkey anti-Rabbit-Alexa Fluor 568	Abcam	Cat#ab175470; RRID: AB_2783823
Goat anti-Mouse IgG1 CF-770	Biotium	Catalog#20254; RRID: AB_10853480
Goat anti-Mouse IgG2a-Alexa Fluor 568	Invitrogen	Cat#A-21134; RRID: AB_2535773
Goat anti-Chicken-Alexa Fluor 488	Invitrogen	Cat#A-11039; RRID: AB_2534096
Goat anti-Mouse-Alexa Fluor Plus 555	Invitrogen	Cat#A-32727; RRID: AB_2633276
Goat anti-Rabbit-Alexa Fluor 488	Invitrogen	Cat#A-11034; RRID: AB_2576217
Bacterial and Virus Strains		
BL21 DE3	Lucigen	Cat#60401
Chemicals, Peptides, and Recombinant Proteins		
Protein-A-HRP	Invitrogen	Cat#101023
Rab34 (WT, L61D, S166N)	This paper	
Anti-GFP Nanobody Alexa Fluor 647	Breslow lab[55]	N/A
GFP Trap	Chromotek	Cat#gta-20

Author Manuscript Author Manuscript Author Manuscript Author Manuscript

REAGENT or RESOURCE	SOURCE	IDENTIFIER
Collagen I	KOKEN	Cat#IPC-50
Cytochalasin D	Sigma Aldrich	Cat#C8273
Dialyzed fetal bovine serum	Gibco	Cat#A3382001
Fluoromount-G mounting medium	Electron Microscopy Sciences	Cat#17984-25
HRV3C protease	Pierce	Cat#88946
Lenti-X Concentrator	Takara Biosystems	Cat#631231
^{32}P orthophosphate	Perkin Elmer	Cat# NEX053H002MC
PEI Max (polyethyleneimine)	Polysciences	Cat#24765-1
ProLong Diamond mounting medium	Thermo Fisher	Cat#P36965
Sodium acrylate	Combi-Blocks	Cat#QC-1489
X-tremeGENE 9	Sigma Aldrich	Cat#6365779001
Experimental Models: Cell Lines		
Mouse: NIH-3T3 [Shh-BlastR;Cas9] cell line	Breslow lab[14]	N/A
Human: RPE1-hTERT cell line	ATCC	Cat#CRL-4000; RRID: CVCL_4388
Dog: MDCK II cell line	Katsuhiko Mikoshiba (ShanghaiTech Univ.)	Cat#RCB5148 (RIKEN BRC)
Dog: MDCK Rab34 KO, Rab36 KO, Rab34/Rab36 DKO cell lines	Fukuda lab[38]	Cat#RCB5133, 35, 46 (RIKEN BRC)
Human: HEK293T cell line	ATCC	Cat#CRL-3216; RRID: CVCL_0063
Oligonucleotides		
Primer: ATCGTTCCATCTCGAAGTCC, Reverse primer for human *RAB34* amplification and sequencing	This study	N/A
Primer: GGGTGTCTTAGAATATAGGAC, Forward primer for human *RAB34* amplification and sequencing	This study	N/A
sgRNA: TTGAACCTCTCCTGCCCAG, sgRNA-A for human *RAB34*	This study	N/A
sgRNA: ATCTCCAAGGTCATTGTGG, sgRNA-B for human *RAB34*	This study	N/A
sgRNA: GAATTACAAGGCTACCAT, sgRNA-A for mouse *Rab34*	This study	N/A
sgRNA: TGGCTCACTGATGCCCTCA, sgRNA-B for mouse *Rab34*	This study	N/A
Recombinant DNA		
pGro7 (GroEL/ES)	Yong Xiong, Yale Univ.	N/A
pGEX-6P-1-Rab34 (WT, L61D, and S166N)	This study	N/A
RAB34 (human) cDNA	GE Healthcare	Cat# MHS6278-202807876
pCW-Tet-LAP-Rab34	This Study	
pCW-Cas9	Addgene	Cat#50661; RRID: Addgene_50661
Lenti-Cas9-Blast	Addgene	Cat#52962; RRID: Addgene_52962
pEF5-FRT-LAP-DEST	Breslow lab[55,56]	N/A
pHR-Pgk-Cas9-BFP	Breslow lab[14]	N/A
pDONR-221	Invitrogen	Cat#12536017
pCW-Pgk-ARL13B-mScarlet-I_Pgk-miRFP-670-Centrin2	This study	N/A

Author Manuscript Author Manuscript Author Manuscript Author Manuscript

REAGENT or RESOURCE	SOURCE	IDENTIFIER
pCW-Pgk-EHD1-mScarlet-I_Pgk-miRFP-670-Centrin2	This study	N/A
pCW-Pgk- mScarlet-I-Rab8a_Pgk-NeoR	This study	N/A
pMCB320-sgRNA_PuroR-T2A-mCherry	Addgene	Cat#89359; RRID: Addgene_89359
pMJ179-sgRNA_PuroR-T2A-BFP	Addgene	Cat#89556; RRID: Addgene_89556
pMD2.G	Addgene	Cat#12259; RRID: Addgene_12259
pRSV-Rev	Addgene	Cat#12253; RRID: Addgene_12253
pMDLg/RRE	Addgene	Cat#12251; RRID: Addgene_12251
pCMV-ΔR-8.91	Bob Weinberg	N/A
pCMV-VSVG	Addgene	Cat#8454; RRID: Addgene_8454
Software and Algorithms		
Nikon Elements AR	Nikon Instruments	RRID: SCR_014329
Fiji (ImageJ)	NIH	RRID: SCR_002285
SmartSEM	Carl Zeiss Microscopy	https://www.zeiss.com/microscopy/int/products/microscope-software/smartsem.html
Atlas engine 5	Carl Zeiss Microscopy	https://www.zeiss.com/microscopy/int/products/microscope-software/atlas.html
DragonFly	Object Research Systems	https://www.theobjects.com/dragonfly/index.html
IMOD	See [57,58]	RRID: SCR_003297
ImageQuant	GE Healthcare	RRID: SCR_014246
Softworx	GE Healthcare	RRID: SCR_019157
Matlab	The Mathworks	RRID: SCR_001622